Behavior of vacancies near edge dislocations in Ni and α-Fe: Positron annihilation experiments and rate theory calculations

Koichi Sato, Toshimasa Yoshiie, Toshitaka Ishizaki,[*] and Qiu Xu

Research Reactor Institute, Kyoto University, Kumatori-cho, Sennan-gun, Osaka, 590-0494, Japan

(Received 23 August 2006; revised manuscript received 20 December 2006; published 14 March 2007)

In order to study behaviors of vacancies near edge dislocations, the lifetime and coincidence Doppler broadening of positron annihilation on Ni and Fe deformed at high speed and low speed were measured. The formation and migration energies and positron annihilation lifetime of vacancies associated with edge dislocations were also calculated. In the experiments, the existence of vacancies associated with edge dislocations, previously predicted by Häkkinen *et al.* and Kamimura *et al.* from calculations, was confirmed. Vacancies were released from the edge dislocations at 573 K in isochronal annealing for 10 hours in Fe. These experimental results were explained by a calculation based on a rate theory. The effect of vacancy diffusion along edge dislocations was also studied, and the obtained results corresponded to those of previous experiments on vacancy self-diffusion along dislocations using the radioactive tracer method.

I. INTRODUCTION

Many important properties in metals can be controlled by means of crystal lattice defects. Vacancies and interstitials are the simplest and most fundamental defects and play an important role in defect structure evolution. They are annihilated at sinks, and dislocations are one of the most important kinds of such sinks. We have believed that point defects near edge dislocations are absorbed easily, which leads to the climb motion of dislocation[1–4] by formation and movement of jogs owing to easy diffusion of point defects along dislocation cores (pipe diffusion).[5–7]

In metals under high-energy particle irradiation, the same number of vacancies and interstitials are formed. Most point defects are absorbed by edge dislocations and a small unbalanced reaction between point defects and dislocations causes void growth (dislocation bias model).[8–12] This model is based on the idea that edge dislocations are perfect sinks for point defects.

There have been reported, however, some experimental results that have made us question the role of dislocations as sinks for point defects. Hidalgo *et al.* performed positron-annihilation-lifetime measurements on Fe deformed under the tensile mode, and obtained a long positron lifetime of 150 ± 4 ps,[13] which was shorter than that of vacancies in the matrix (180 ps).[14] They concluded that the lifetime should be assigned to positron annihilation at screw and edge dislocations. Häkkinen *et al.* first indicated the existence of vacancies associated with the dislocation line.[15,16] They calculated the positron lifetimes of edge dislocations and vacancies on an edge dislocation line in Al and Cu. The obtained values were 114 ps and 166 ps, respectively, in Cu. Kamimura *et al.* also calculated the same positron lifetimes in Fe.[17] The obtained values were 117 ps and 140 ps, respectively. They pointed out that the positron lifetime of 150 ps obtained by Hidalgo *et al.* could not be due to the dislocation line but rather the lifetime of vacancies on the dislocation line. Diffusion of point defects along edge dislocations in fcc metals has been reported.[18–24] The dislocations were extended and a vacancy at the edge of a partial dislocation had

the form of a distorted hexagon in the (111) plane.[20] The formation energy of a vacancy at the edge of a partial dislocation, calculated using the *N*-body potential, decreased from the bulk value of 1.19 eV to 0.97 eV in Cu.[23] From a molecular dynamics simulation at high temperature, the vacancy migration energy near the partial dislocation decreased only by 0.75 eV compared with the bulk value of 0.98 eV in Cu.[18,23] Owing to the extension of dislocations, the trajectories of the vacancy migration were involved not only in the partial dislocations but also in the stacking fault region.[20] For this reason, vacancy diffusion in fcc metals along partial dislocation pairs is not expected to be particularly fast.[20]

In this paper, we report on the vacancy trapping and detrapping behavior in dislocations, which is different from the formation and absorption of point defects by jogs. First, the existence of vacancies trapped in dislocations and the detrapping behaviors thereof during isochronal annealing were demonstrated in deformed Fe and Ni by experiments. We performed positron-annihilation-lifetime measurement and coincidence Doppler broadening (CDB) of positron annihilation measurement on Fe and Ni deformed at high speed and low speed. After that, we investigated the annealing behavior of vacancies trapped near dislocations. Next, the strength of vacancy trapping in dislocations and the effect of vacancy pipe diffusion were studied by computer simulation. The formation energy and the migration energy of vacancies near perfect edge dislocations in α-Fe and extended dislocations in Ni were calculated employing the *N*-body potential, and the energy calculation of the model lattice was performed employing the static method.[25,26] The positron lifetime of vacancies near dislocation cores was also calculated, using a method proposed by Puska and Nieminen.[27] Results obtained with these calculations were compared with experimental results.

II. POSITRON ANNIHILATION MEASUREMENT

A. Experimental procedure

Pure Fe (99.99%) and pure Ni (99.99%) specimens were measured to be approximately 3 mm in diameter and 0.1 mm

in thickness. The specimens of Fe were annealed at 1223 K for 0.5 hours followed by quenching into water, and those of Ni were annealed at 1173 K for 1 hour in a high vacuum of less than 1.0×10^{-4} Pa. The specimens were polycrystals, and the average grain size was 25 μm for Fe and 50 μm for Ni. The high- and low-speed deformation experiments were carried out using an impact deformation apparatus and a conventional oil press at the Hiroshima Institute of Technology. The strain rates during high- and low-speed deformation experiments were 4.3×10^5 s and 67 s, respectively. The strain for every specimen was approximately 30%. Annealing experiments were performed on the deformed specimens at intervals of 100 K and 50 K up to 873 K and 723 K for Fe and Ni, respectively. The annealing time at each temperature was 10 hours. Positron-annihilation-lifetime measurement and CDB measurement of positron annihilation were carried out before and after each annealing process.

A ^{22}Na source of positrons was used for the positron annihilation lifetime and CDB measurements. The radioactivity of the source for the lifetime measurements was approximately 30 μCi (1.1 MBq) and that for the CDB measurements was approximately 20 μCi (0.7 MBq). The system employed for positron annihilation lifetime measurements in this study was a conventional fast-fast circuit with two BaF$_2$ scintillators. The time resolution of the system was approximately 190 ps at full width at half-maximum (FWHM). The positron lifetime spectra were analyzed using the Resolution and Positronfit programs.[28] In order to measure CDB spectra, two Ge detectors were placed at 180° with respect to one another with a spacing of 400 mm therebetween. The overall energy resolution of the two Ge detectors was 1.6 keV at FWHM for 661.6 keV γ rays from a ^{137}Cs standard radiation source. All positron annihilation experiments were performed at room temperature. Mean lifetime, long lifetime, and long lifetime intensity obtained from the positron annihilation lifetime measurements correspond to the total amount of residual defects, the size of vacancy clusters, and the amount of vacancy clusters, respectively. The S-parameter ratio obtained from CDB measurements is defined as the ratio of the counts in the low-momentum region (Fe, less than 4.0×10^{-3} mc; Ni, less than 5.0×10^{-3} mc) relative to the total counts, and corresponds to the total amount of vacancy-type defects.

B. Results and discussion

Figures 1 and 2 show a comparison of the isochronal annealing behaviors of the positron annihilation lifetime and S-parameter ratio from CDB measurements in pure Ni for high- and low-speed deformations, respectively. The size of vacancy clusters and the amount of vacancy-type defects were larger after high-speed deformation than after low-speed deformation. This is the same result as reported by Kiritani *et al.*[29–32] In addition, the complete recovery temperature of the specimen deformed at low speed was higher than that of the specimen deformed at high speed. This leads to the conclusion that recovery of vacancy-type defects introduced by high-speed deformation was faster. This conclusion was explained by the characteristic difference between
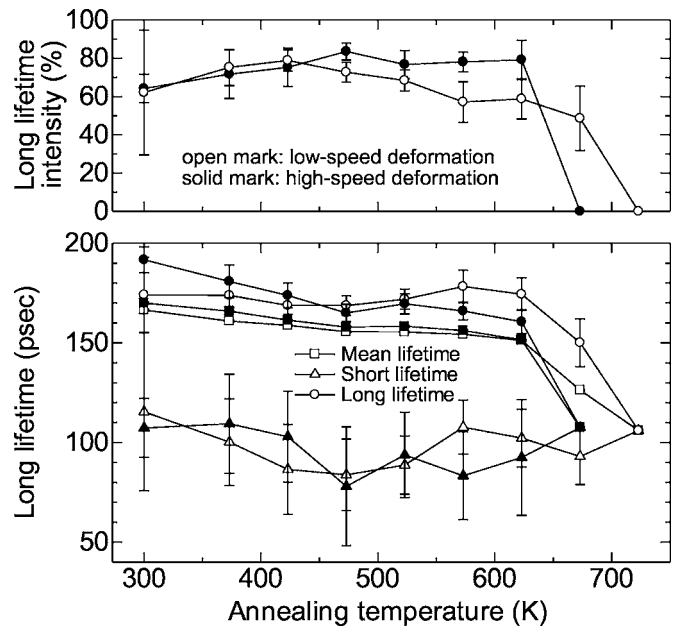
FIG. 1. Comparison of isochronal annealing behaviors of positron annihilation lifetime and long lifetime intensity in pure Ni for high- and low-speed deformation (annealing time, 10 hours; bulk lifetime, 110 ps).

dislocation structures derived from the transmission electron microscopy, i.e., dislocations introduced by high-speed deformation were distributed much more homogeneously than those introduced by low-speed deformation,[29–32] and they act as more effective sinks for vacancies. The annealing behaviors of mean lifetime and S-parameter ratio were almost the same.

Figures 3 and 4 show a comparison of the isochronal annealing behaviors of the positron annihilation lifetime and S-parameter ratio from CDB measurements in pure Fe for high- and low-speed deformations, respectively. The size of
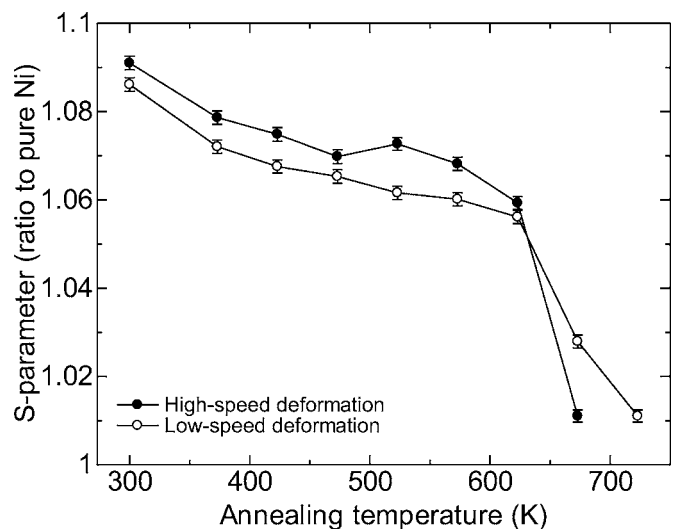
FIG. 2. Comparison of isochronal annealing behaviors of S-parameter ratio in pure Ni for high- and low-speed deformation (annealing time, 10 hours).
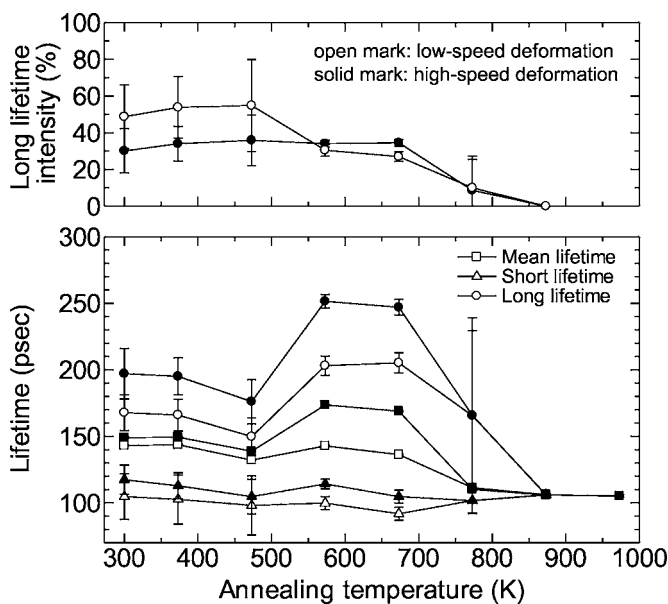
FIG. 3. Comparison of isochronal annealing behaviors of positron annihilation lifetime and long lifetime intensity in pure Fe for high- and low-speed deformation (annealing time, 10 hours; bulk lifetime, 110 ps).

vacancy clusters and the amount of vacancy-type defects were larger after high-speed deformation than after low-speed deformation. The complete recovery temperature was the same in both cases.

The long lifetime of 168 ps in the low-speed deformed Fe was assigned to a combining lifetime of monovacancies in a matrix (180 ps) (Ref. 14) and vacancies on an edge dislocation line (140 ps).[17] The long lifetime of 197 ps in the high-speed deformed Fe was also assigned to a combining lifetime of monovacancies, vacancy clusters (2–3 vacancies), and vacancies on the edge dislocation line. After annealing at 473 K, the long lifetime was shorter than that of vacancies in the matrix. A number of the vacancies in the matrix were
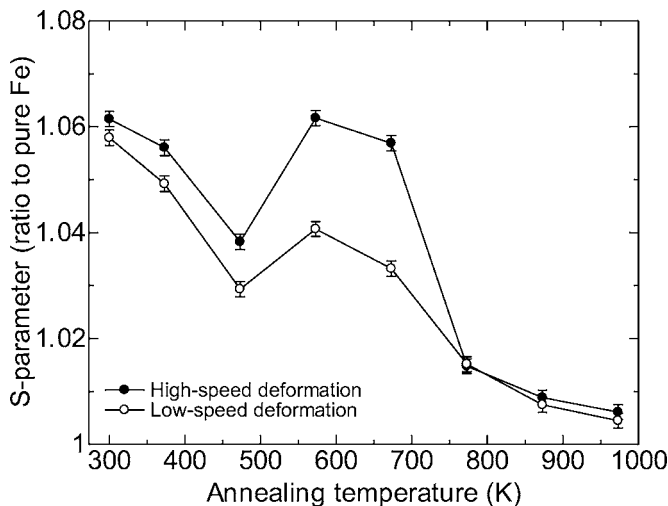
FIG. 4. Comparison of isochronal annealing behaviors of S-parameter ratio in pure Fe for high- and low-speed deformation (annealing time, 10 hours).

TABLE I. Calculated positron annihilation lifetimes of vacancies and their clusters associated with edge dislocations in α-Fe. When three vacancies lie on a dislocation line, the vacancies shrink in size and their structure becomes the same as that of the jogs after relaxation by the static method.

		Positron annihilation lifetime (psec)
one vacancy		144
two vacancies		153
three vacancies		117
jogs		117

considered to have migrated to the dislocation line without annihilation, because the intensity of the long lifetime did not change. Table I shows the calculated positron annihilation lifetime of vacancies and their clusters associated with edge dislocations in α-Fe. The lifetime of the jogs of edge dislocations is 117 ps,[17] which is almost equal to that of edge dislocations and is too short to allow separation of the lifetime component from the matrix component. If vacancies are annihilated at jogs of the edge dislocations, the long lifetime will further decrease. After annealing at 573 K, the long lifetime, mean lifetime, and S-parameter ratio increased. In particular, the intensity of 35% was constant in the high-speed deformed Fe during annealing between 373 K and 673 K. Most vacancy clusters were not annihilated and grew by means of the absorption of vacancies. For this growth of vacancy clusters without a change in concentration caused by isochronal annealing, vacancies must be formed somewhere at 573 K. However, many vacancies cannot be generated from grain boundaries or jogs of the edge dislocations at thermal equilibrium at 573 K or 673 K (see the following section). The only possible source of vacancies is the release of vacancies trapped in the edge dislocations. Vacancies were detrapped from edge dislocations, aggregated in the matrix, and formed larger vacancy clusters at 573 K.

In Ni, the increases of the long lifetime, mean lifetime, and S-parameter ratio were less noticeable than in Fe after annealing at 573 K. Because edge dislocations in fcc metals are extended, the strain of perfect edge dislocations is higher than that of extended dislocations. Therefore, emission of vacancies trapped in dislocations was more significant in Ni than in Fe.

Although the specimens used in these experiments were polycrystals, consideration of the effect of grain boundaries was omitted, because, as mentioned in the following section, the range of interaction between the edge dislocations and the vacancies was narrow (five atomic distances at most) and few vacancies are formed from the grain boundaries at 573 K or 673 K. Consideration of the effect of screw dislocations was also omitted, because the change in volume caused by screw dislocations was too small to affect the behavior of vacancies.

In this section, the existence of vacancies trapped in edge dislocations and the detrapping of the vacancies from the
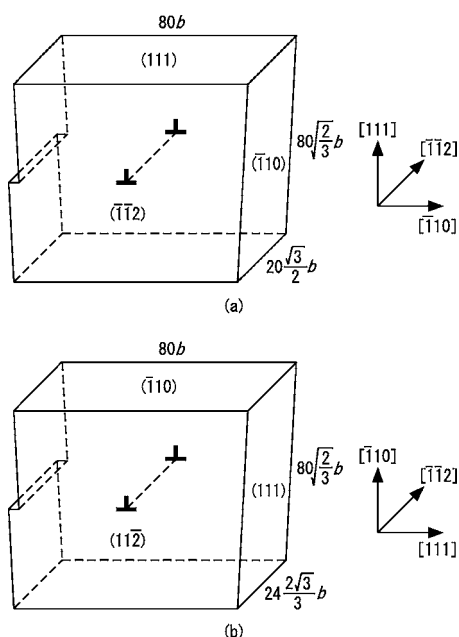
FIG. 5. Size and orientation of model lattice, (a) Ni and (b) Fe (*b* denotes atomic distance). The number of atoms used in this calculation was 128 000 and 153 600 for Ni and Fe, respectively.

edge dislocations were confirmed. In Sec. III, the formation and migration energies and the positron annihilation lifetime of vacancies near the edge dislocations were calculated, and the strength of vacancy trapping in dislocations and the effect of vacancy pipe diffusion were estimated. In comparison with the experiments, the validity of the mechanism of vacancy trapping and detrapping in dislocations derived from the computer simulation was examined.

III. SIMULATION OF VACANCY BEHAVIORS NEAR EDGE DISLOCATIONS

A. Method of calculation

1. Calculation model

The effective medium theory (EMT) potential for Ni fitted by Jacobsen *et al.*[33] and the Ackland-Bacon-Calder-Harry (ABCH) potential for α-Fe (Ref. [34]) were used for computer simulation. Figures 5(a) and 5(b) show the size and orientation of the model lattice we employed in Ni and Fe, respectively. The number of atoms used in this calculation was 128 000 and 153 600 for Ni and Fe, respectively. We defined the $[\bar{1}10]$, $[11\bar{2}]$, and $[\bar{1}11]$ directions as the *x*, *y*, and *z* axes in Ni, and the $[111]$, $[11\bar{2}]$, and $[\bar{1}10]$ directions as the *x*, *y*, and *z* axes in Fe, respectively. The edge dislocation line parallel to the *y* axis was introduced at the center of the model lattice by displacing the atoms according to elasticity theory. The Burgers vector was $a/2[\bar{1}10]$ and $a/2[111]$ in Ni and Fe, respectively, where *a* was the lattice constant. A periodic boundary condition for the *y* axis and the fixed boundary conditions at surfaces perpendicular to the *x* axis and *z* axis were employed. The atomic positions at the fixed boundary were also determined according to the elasticity theory. The
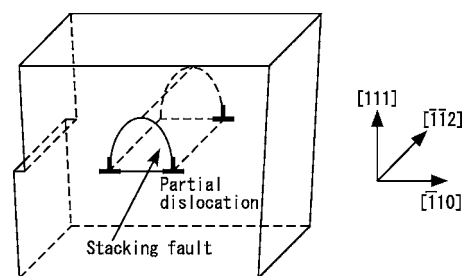
FIG. 6. Partial dislocations induced by relaxation of perfect edge dislocations.

lattice was relaxed using the static method, which did not take into account the effects of temperature.

A perfect edge dislocation in Ni extended into two partial dislocations with the relaxation. The edge dislocation obtained in this calculation separated on the slip plane, and the stacking fault formed by the two partial dislocations was recovered approximately 10 layers above the slip plane, as shown in Fig. 6. For the simulation of vacancy migration in the extended dislocation, this model lattice was used. Distance between the two partial dislocations was 8–9 atomic distance in Ni. The stacking fault energy was approximately 100 mJ/m² . This value corresponded to the experimental values of 100–200 mJ/m² in Ni.[35]

2. Calculation of formation energy and migration energy of vacancies

The formation energy of vacancies was determined as follows. First, we calculated the total energy of the relaxed model lattice with a dislocation (E_1) before introducing vacancies. Next, we introduced vacancies into the relaxed model lattice, and calculated the total energy after relaxation (E_2). A vacancy was introduced by removing one atom from the perfect lattice. Thus, the vacancy formation energy E_v^f was obtained as the difference between E_1 and the sum of E_2 and the cohesive energy E_c, which was obtained by dividing the total energy of the perfect lattice by the number of atoms,

$$E_v^f = E_2 + E_c - E_1. \tag{1}$$

When vacancies migrate to a neighboring site, they must pass through the saddle point. So, the migration energy was determined as the difference between the total energy of the model lattice with an atom at the lattice point before the migration and that with the atom at the saddle point. For example, in a vacancy, the migration from position (*A*) to position (*B*) in Fig. 7 is equivalent to the migration of an atom from position (*B*) to position (*A*). The atom was placed at each of approximately 20 points along a line segment *AB*, and was relaxed at each point only in the plane perpendicular to the line segment *AB*, and the other atoms were relaxed freely. The saddle point was defined as the place where the total energy of the model lattice is at its maximum for this particular migration route. Even if the nudged elastic band method is used, which is more reliable than the present calculation method for the saddle point search, the vacancy migration energies obtained are not markedly different from
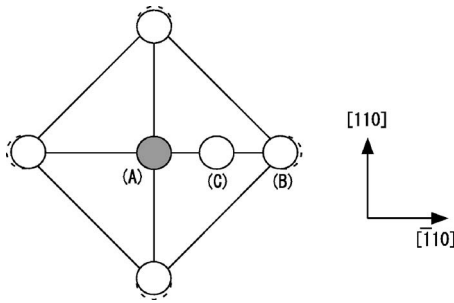
FIG. 7. Migration of vacancy. (*A*) is a vacancy site, (*B*) is the first nearest-neighbor atom that will migrate to the vacancy site, and (*C*) is the saddle point. Dotted circles and solid circles denote the atomic position before and after relaxation, respectively.

those obtained in our calculation. This is because the vacancy migration path is simple.

The formation energy and migration energy of vacancies in the perfect lattice calculated using these methods and their experimental values are shown in Table II. The migration energy calculated in the present study corresponds to that obtained by the molecular dynamics simulation.[34] The experimental vacancy migration energies in Ni and α-Fe greatly differed between low and high purity.

3. Positron annihilation lifetime calculation

To calculate the positron lifetime the Schrödinger equation must be solved to determine the positron wave function at defect sites, as carried out in the method developed by Puska and Nieminen.[27] In this calculation, the potential for a positron must be given. This consists of a Coulomb potential from nuclei and electrons and a correlation potential between a positron and an electron. The Coulomb potential was constructed by superposition of the atomic wave function given by Herman and Skillman[43] and the correlation potential was

TABLE II. Calculated and experimental formation and migration energies of vacancies in perfect lattice. The EMT potential for Ni (Ref. 33) and the ABCH potential for α-Fe (Ref. 34) were used. The experimental vacancy migration energy in Ni and α-Fe varied markedly between low- and high-purity samples.

	Formation energy (eV)		Migration energy (eV)	
	Present study	Experiment	Present study	Experiment
Ni	1.90	1.74[a]	1.17	1.25 (low purity)[b]
				1.03 (high purity)[c]
α-Fe	1.70	1.79[d]	0.78	1.24 (low purity)[e]
				0.55 (high purity)[f,g]

[a]Reference 36.
[b]Reference 37.
[c]Reference 38.
[d]Reference 39.
[e]Reference 40.
[f]Reference 41.
[g]Reference 42.

given by Boronski and Nieminen[44] based on the local density approximation (LDA). To solve the Schrödinger equation the numerical method given by Kimball and Shortley[45] was used. Enhancement factors corresponding to *d* electrons arising from the positron-electron correlation effects Γ_d were determined so that the calculated lifetime in the matrix agreed with the experimental results. In this study, Γ_d for Ni and Fe was 1.75 and 2.19, respectively, and the matrix lifetime was 110 ps in both metals.[14,17,46] The positron lifetime calculations were performed for relaxed vacancies obtained by the above static method.

B. Results

Figures 8 and 9 show the structure of partial dislocations in Ni and perfect dislocation in α-Fe, respectively. A vacancy was introduced at position "*V*0," "*RT*1"–"*RT*4," "*LT*1"–"*LT*3," "*UP*1"–"*UP*4," "*LW*1"–"*LW*5" or "*CT*" (only in the case of partial dislocations). The vacancy formation energy at each position, the energy required for vacancy migration between the positions, and the positron annihilation lifetime were calculated. "*P*1" and "*P*2" denote two routes of vacancy migration along the dislocation line, so-called pipe diffusion. "*CT*" denotes the center of the stacking fault ribbon.

1. Ni

Figure 10 shows the results of vacancy formation energy, migration energy, and positron annihilation lifetime in Ni obtained by computer simulation. The vacancy formation energy at position "*V*0" was lowest in a direction perpendicular to the slip plane. The lowest formation energy was at position "*LT*2," where misalignment of atomic position caused by partial dislocations begins to occur. Vacancy migration energy in the Burgers vector direction was lower than that in other directions. In a direction perpendicular to the slip plane, the energy required to migrate to the dislocation core was lower than the energy required to move away from the dislocation core. On the basis of these results, it is considered that vacancies can easily migrate to a boundary between a perfect lattice region and partial dislocations on the slip plane. The vacancy migration energy for the pipe diffusion was low in the migration route of "*P*2." In the pipe diffusion, vacancies mainly migrate through the route of "*P*2," and diffuse to the stacking fault region. In the region far from the partial dislocations, the migration energy of the route "*P*1" decreased and that of "*P*2" increased to 1.02 eV, as shown in "*CT*" of Fig. 10. This means that the migration energy of pipe diffusion was lower than that of the bulk diffusion of 1.17 eV. The result of the molecular dynamics calculation[20] is associated with diffusion. The positron annihilation lifetime of vacancies decreased in the compressional side and increased in the dilatational side, and the change in lifetime was approximately ±10 ps compared with the lifetime in the matrix.

2. α-Fe

Figure 11 shows the results of vacancy formation energy, migration energy, and positron annihilation lifetime in α-Fe
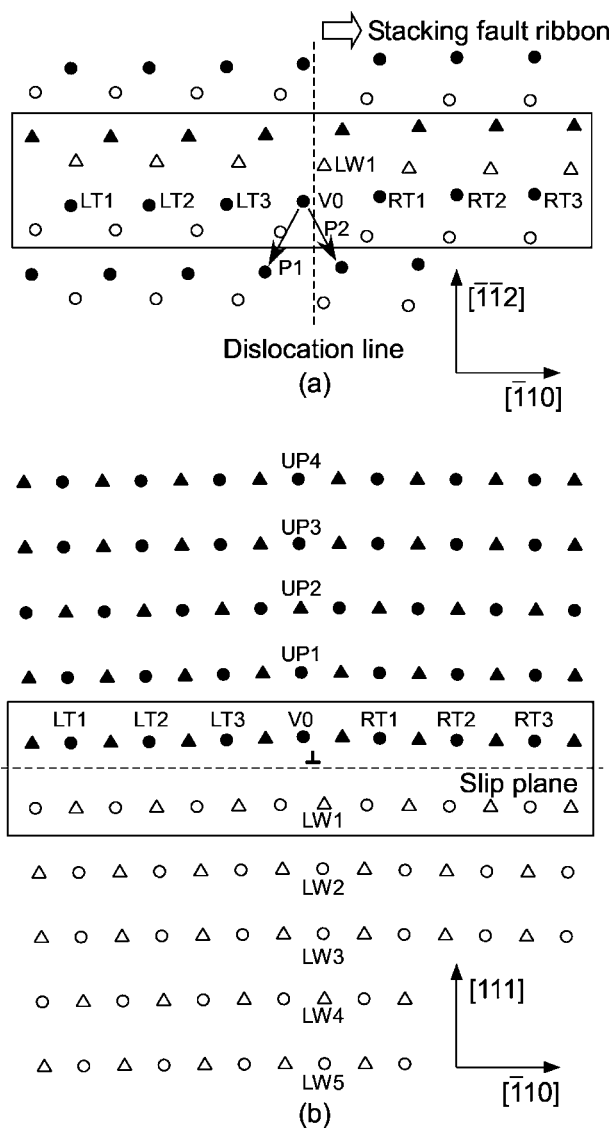
FIG. 8. Structure of partial dislocations in Ni. Solid and open marks denote atoms above and below the slip plane, respectively. (a) is the top view and (b) is the side view of the model lattice. The square frame in each figure corresponds to the drawing area in the other figure. Triangular and circular marks denote higher and lower atoms in the $[\bar{1}\bar{1}2]$ direction, respectively. A vacancy was introduced at each of the positions "$V0$," "$RT1$"–"$RT3$," "$LT1$"–"$LT3$," "$UP1$"–"$UP4$," and "$LW1$"–"$LW5$." "$P1$" and "$P2$" denote two routes of vacancy migration along the dislocation line, so-called pipe diffusion.

obtained by computer simulation. The vacancy formation energy at position "$V0$" was lowest. Generally, the formation energy was low in the compressional side, and high in the dilatational side. In the same way as Ni, the vacancy migration energy in the Burgers vector direction was lower than that in the other directions. The energy required to migrate to the dislocation core was lower than the energy required to move away from the dislocation core. On the basis of these results, it is considered that vacancies can easily migrate to the dislocation core. The vacancy migration in directions "$P1$" and "$P2$" denote migrations to second and first nearest
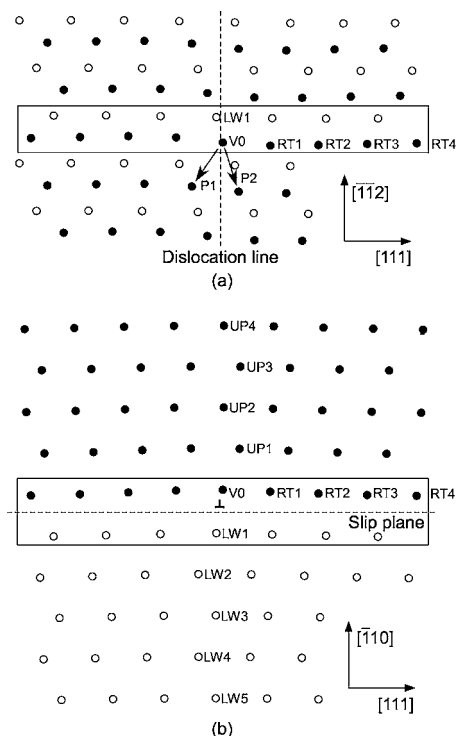
FIG. 9. Structure of partial dislocations in Fe. Solid and open marks denote atoms above and below the slip plane, respectively. (a) is the top view and (b) is the side view of the model lattice. The square frame in each figure corresponds to the same area. A vacancy was introduced at each of the positions "$V0$," "$RT1$"–"$RT4$," "$UP1$"–"$UP4$," and "$LW1$"–"$LW5$." "$P1$" and "$P2$" denote two routes of vacancy migration along the dislocation line, so-called pipe diffusion.

sites, respectively. The vacancy migration energy in direction "$P1$" was lower than that in direction "$P2$," and, in the perfect lattice, the former was higher than the vacancy migration energy. The vacancy migration energy to the second nearest site was 3.54 eV in the perfect lattice, and the perfect dislocations caused a marked decrease thereof. The positron annihilation lifetime of vacancies decreased up to 144 ps in the compressional side, and increased in the dilatational side. Results of the vacancy formation energy and the positron annihilation lifetime were in close agreement with the results of Ref. 17.

C. Discussion

1. Strength of vacancy trapping

Our calculation in Fe clearly showed that vacancies on dislocation lines did not move along the dislocation line and were not annihilated at room temperature (see following section). When vacancies are associated with dislocations, vacancies can easily migrate near a dislocation core on the slip plane. If vacancies are detrapped from dislocations at elevated temperatures, vacancies move away from the dislocations perpendicular to the dislocation line on the slip plane. In order to compare these calculation results with the experimental results, an analysis using a rate equation was per-
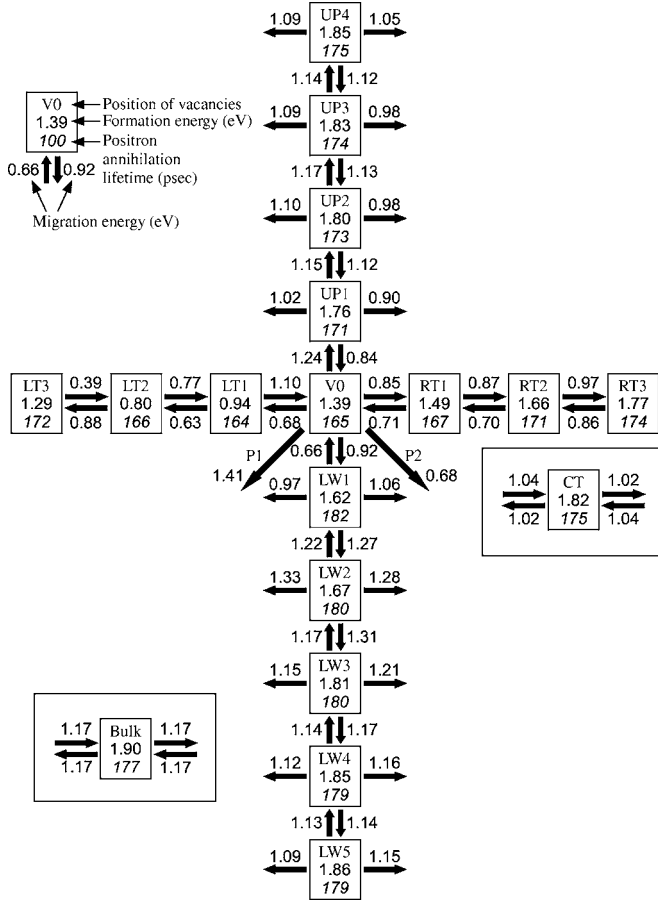
FIG. 10. Vacancy formation energy, migration energy, and positron annihilation lifetime in Ni obtained by computer simulation. "*CT*" denotes center of stacking fault ribbon.

FIG. 11. Vacancy formation energy, migration energy, and positron annihilation lifetime in α-Fe obtained by computer simulation.

formed in Fe. The vacancy concentrations at "$V0$," "$RT1$," "$RT2$," "$RT3$," and "$RT4$" are expressed as C_0, C_1, C_2, C_3, and C_4, respectively. The vacancy concentration outside of "$RT4$," expressed as C_5, was assumed to be not influenced by the dislocations and constant. The variations of the above parameters at time t are

$$\frac{dC_0}{dt} = -Z_1(1-C_1)M_{01}C_0 + Z_1(1-C_0)M_{10}C_1, \quad (2)$$

$$\frac{dC_1}{dt} = -Z_2(1-C_0)M_{10}C_1 - Z_2(1-C_2)M_{12}C_1$$
$$+ Z_2(1-C_1)M_{01}C_0 + Z_2(1-C_1)M_{21}C_2, \quad (3)$$

$$\frac{dC_2}{dt} = -Z_2(1-C_1)M_{21}C_2 - Z_2(1-C_3)M_{23}C_2$$
$$+ Z_2(1-C_2)M_{12}C_1 + Z_2(1-C_2)M_{32}C_3, \quad (4)$$

$$\frac{dC_3}{dt} = -Z_2(1-C_2)M_{32}C_3 - Z_2(1-C_4)M_{34}C_3$$
$$+ Z_2(1-C_3)M_{23}C_2 + Z_2(1-C_3)M_{43}C_4, \quad (5)$$

$$\frac{dC_4}{dt} = -Z_2(1-C_3)M_{43}C_4 - Z_2(1-C_5)M_{45}C_4$$
$$+ Z_2(1-C_4)M_{34}C_3 + Z_2(1-C_4)M_{54}C_5, \quad (6)$$

$$\frac{dC_5}{dt} = 0, \quad (7)$$

where $Z_1(1-C_n)$ and $Z_2(1-C_n)$ ($n=0-5$) are the numbers of sites for the reaction and M_{ij} is the mobility from site i to site j. Z_1 and Z_2 are 2 and 1, respectively, because the calculation model is one-dimensional and symmetric with respect to the dislocation core. M_{ij} is expressed as $v_0 \exp(-E_{ij}/kT)$, where v_0 is frequency of lattice vibration, E_{ij} is the migration energy from the site i to the site j, k is the Boltzmann constant, and T is absolute temperature. First, the vacancy concentrations were calculated at room temperature using an initial condition assuming thermal equilibrium. For the 10 hour simulation of isochronal annealing, the vacancy concentrations at 373 K for 10 hours were calculated using the results

TABLE III. Change in vacancy concentration near dislocation core in 1 hour simulation of isochronal annealing in Fe. The vacancy concentrations at "V0," "RT1," "RT2," "RT3", and "RT4" in Fig. 8 are expressed as C_0, C_1, C_2, C_3, and C_4, respectively. The vacancy concentration outside of "RT4" is expressed as C_5. "—" denotes that vacancy concentration is almost zero. "Total" denotes the sum of the vacancy concentrations near the dislocation core ($C_0+2C_1+2C_2+2C_3+2C_4$). In the first case, all trapped vacancies exist in the dislocation core and the vacancy concentration C_5 is at thermal equilibrium [$C_0=1, C_1=C_2=C_3=C_4=0, C_5=\exp(-E_f/kT)$]. In the second case, no vacancies are trapped in the dislocation, and the vacancy concentration C_5 is that produced by the deformation ($C_0=C_1=C_2=C_3=C_4=0, C_5=1\times10^{-10}$). It was assumed that C_5 was constant during annealing. In the third and fourth cases, the normalized migration energies of vacancies near the edge dislocations were used.

Temperature	Vacancy concentration						
	C_0	C_1	C_2	C_3	C_4	C_5	Total
First case							
300 K	0.71	0.14	1.0×10^{-6}	6.7×10^{-10}	1.4×10^{-12}	2.9×10^{-29}	1.0
373 K	0.61	0.15	1.2×10^{-5}	3.1×10^{-8}	2.2×10^{-10}	1.1×10^{-23}	0.91
473 K	4.0×10^{-3}	7.2×10^{-4}	3.6×10^{-7}	3.4×10^{-9}	6.8×10^{-11}	7.8×10^{-19}	5.5×10^{-3}
573 K	2.7×10^{-8}	6.7×10^{-9}	1.3×10^{-11}	2.7×10^{-13}	1.0×10^{-14}	1.0×10^{-15}	4.1×10^{-8}
673 K	3.6×10^{-7}	1.1×10^{-7}	5.2×10^{-10}	2.0×10^{-11}	1.3×10^{-12}	1.9×10^{-13}	5.8×10^{-7}
Second case							
300 K	5.1×10^{-4}	3.4×10^{-5}	2.1×10^{-10}	1.4×10^{-13}	1.2×10^{-15}	1.0×10^{-10}	5.8×10^{-4}
373 K	1.8×10^{-3}	2.1×10^{-4}	1.4×10^{-8}	3.7×10^{-11}	2.6×10^{-13}	1.0×10^{-10}	2.3×10^{-3}
473 K	0.13	2.6×10^{-2}	1.4×10^{-5}	1.3×10^{-7}	2.5×10^{-9}	1.0×10^{-10}	0.18
573 K	2.4×10^{-3}	5.8×10^{-4}	1.1×10^{-6}	2.3×10^{-8}	9.2×10^{-10}	1.0×10^{-10}	3.6×10^{-3}
673 K	1.9×10^{-4}	5.8×10^{-5}	2.8×10^{-7}	1.1×10^{-8}	6.7×10^{-10}	1.0×10^{-10}	3.1×10^{-4}
Third case							
300 K	0.63	0.20	5.1×10^{-5}	2.3×10^{-7}	3.2×10^{-9}	2.9×10^{-29}	1.0
373 K	1.4×10^{-15}	2.9×10^{-16}	3.1×10^{-19}	4.0×10^{-21}	1.3×10^{-22}	1.1×10^{-23}	2.0×10^{-15}
473 K	—	—	—	—	—	—	—
573 K	—	—	—	—	—	—	—
673 K	—	—	—	—	—	—	—
Fourth case							
300 K	0.59	0.17	4.2×10^{-5}	1.9×10^{-7}	2.6×10^{-9}	1.0×10^{-10}	0.93
373 K	1.2×10^{-2}	2.5×10^{-3}	2.7×10^{-6}	3.5×10^{-8}	1.1×10^{-9}	1.0×10^{-10}	1.7×10^{-2}
473 K	2.5×10^{-4}	7.2×10^{-5}	3.3×10^{-7}	1.1×10^{-8}	7.1×10^{-10}	1.0×10^{-10}	3.9×10^{-4}
573 K	1.9×10^{-5}	6.9×10^{-6}	8.0×10^{-8}	4.7×10^{-9}	5.1×10^{-10}	1.0×10^{-10}	3.3×10^{-5}
673 K	3.1×10^{-6}	1.3×10^{-6}	3.0×10^{-8}	2.6×10^{-9}	4.0×10^{-10}	1.0×10^{-10}	5.8×10^{-6}

at room temperature as the initial condition. The same calculation was performed at intervals of 100 K up to 673 K. Four cases were considered, and obtained results are shown in Table III.

In the first case, all the trapped vacancies exist in the dislocation core and the vacancy concentration C_5 is a thermal equilibrium value. Therefore, the initial condition ($t=0$) is $C_0=1, C_1=C_2=C_3=C_4=0, C_5=\exp(-E_f/kT)$ (E_f, vacancy formation energy in the matrix). At room temperature and at 373 K, almost all vacancies were associated with the dislocations. At temperatures above 573 K, almost all vacancies were detrapped.

In the second case, no vacancies are trapped in the dislocation, and the vacancy concentration C_5 is that produced by the deformation. The initial condition is $C_0=C_1=C_2=C_3=C_4=0, C_5=1\times10^{-10}$. The vacancy concentration $C_5=1\times10^{-10}$ was obtained in the following way. The dislocation density generated by the strain ε of 30% is 10^{11} cm^2.[47] The density of Fe atoms is 8.18×10^{22} cm^3. The concentration of

atoms existing in the dislocation core is $(10^{11}/b)/8.18\times10^{22}=4.85\times10^{-5}$ (b, atomic distance in Fe). The concentration of single vacancies produced by the high-speed deformation is given as 2.2×10^{-6} ($=5\times4.39\times10^{-7}$, see Table IV). The concentration of vacancies existing near the dislocation core is approximately 1×10^{-10}. It was assumed that C_5 was constant during annealing. The vacancies induced by the deformation migrated to the dislocation line up to 473 K. The highest vacancy concentration at the dislocation core was 0.13, and this means that vacancies are trapped every eight atoms along the dislocation line. Thereafter the vacancies were released.

Using the ABCH potential, the vacancy migration energy in the matrix was determined to be 0.78 eV. This value was higher than the one obtained experimentally for high-purity Fe [0.55 eV (Refs. 39 and 40)]. The reason we obtained high values in our calculation is that we did not tune the potential to fit the migration energy. In the third and fourth cases, the rate equation was calculated using the normalized migration

TABLE IV. Values of constants for calculation of defect concentration in Fe.

Lifetime (ps)	Number of vacancies n	Radius of traps R (m)	Capture probability μ	Trapping rate κ	Defect concentration C
200	2	1.78×10^{-10}	3.79×10^{15}	1.95×10^{9}	5.14×10^{-7}
250	5	2.41×10^{-10}	5.15×10^{15}	2.41×10^{9}	4.68×10^{-7}

energies of vacancies near the edge dislocations, which were multiplied by the ratio of the experimental vacancy migration energy in the matrix (0.55 eV) to one obtained using the ABCH potential (0.78 eV). The initial condition was the same as that used in the first and second cases. From the results of the third case, it was determined that vacancies were detrapped after annealing at 373 K for 10 hours. In the fourth case, it was observed that vacancies were already trapped in the dislocation core at 300 K, and vacancies were detrapped at above 373 K. The strength of vacancy trapping depends on the vacancy migration energy in the matrix.

The vacancy migration energy depends on the purity of the specimens, as shown in Table II, i.e., the strength of the vacancy trapping depends on the purity of the specimens. The purity of the specimens used in this experiment was 99.99%, which is lower than that of the high-purity Fe used in the experiments of Refs. 41 and 42 (99.999%). The third and fourth cases are considered to be simulations of vacancy behaviors near edge dislocations in high-purity Fe, and it is impossible to detect detrapping at above room temperature. Therefore, by comparison with experimental results, it was concluded that the second case was the most suitable. This means that, in Fe of 99.99% purity, the actual activation energy is near 0.78 eV, due to the effect of impurities.

2. Estimation of defect concentration and effect of pipe diffusion

The trapping of positrons in vacancy clusters competes with their annihilation in the bulk. If only one type of trap is present, the following kinetic equations from a simple trapping model[48–50] can describe the annihilation of positrons in the defect-free bulk concentration (n_b) and at defects (n_d),

$$\frac{d}{dt} n_b(t) = -\lambda_b n_b - \kappa n_b, \tag{8}$$

$$\frac{d}{dt} n_d(t) = -\lambda_d n_d + \kappa n_b, \tag{9}$$

where κ is the trapping rate and λ_b and λ_d are the annihilation rates in the bulk and at defects, respectively. The starting condition at time $t=0$ for the number of positrons in the bulk and at defects are $n_b(t=0)=1$ and $n_d(t=0)=0$, respectively. The solution to these equations can be easily obtained. The normalized positron lifetime spectrum $n(t)$ is the summation of two exponential components,

$$n(t) = I_1 \exp\left(-\frac{t}{\tau_1}\right) + I_2 \exp\left(-\frac{t}{\tau_2}\right). \tag{10}$$

The lifetimes are written as

$$\tau_1 = (\lambda_b + \kappa)^{-1} = \lambda_1^{-1}, \tag{11}$$

$$\tau_2 = \lambda_d^{-1} = \lambda_2^{-1}, \tag{12}$$

and the relative intensities are

$$I_1 = 1 - I_2, \tag{13}$$

$$I_2 = \kappa(\lambda_b - \lambda_d + \kappa)^{-1}. \tag{14}$$

The trapping rate is derived from the above equations as

$$\kappa = \frac{I_2}{I_1}(\lambda_b - \lambda_2) = I_2(\lambda_1 - \lambda_2). \tag{15}$$

The trapping rate can also be written as

$$\kappa = \mu C, \tag{16}$$

where μ is the capture probability and C is the defect concentration. The capture probability is calculated from the diffusion model as

$$\mu = \frac{4\pi R D}{\Omega} \tag{17}$$

(Ref. 27), where R is the radius of traps, D is the diffusion coefficient (2×10^{-5} m^2/s), and Ω is the atomic volume (1.178×10^{-29} m^3 in Fe, the volume of the unit cell was divided into two). The radius of traps is approximately derived from

$$\frac{4\pi}{3} R^3 = n\Omega, \tag{18}$$

where n is the number of vacancies comprising the vacancy cluster.

The concentration of vacancy clusters in Fe was calculated using these equations. The lifetime of the high-speed deformed Fe was changed from approximately 200 ps to approximately 250 ps by 573 K annealing. The vacancy clusters consisted of two vacancies before annealing and five vacancies after 573 K annealing. Table IV shows values used for the calculation mentioned above. The defect concentration was approximately 5×10^{-7}.

The lowest migration energy for pipe diffusion is 0.97 eV ("P1" in Fig. 11) in Fe. If vacancies migrate only in the direction "P1," they move away from the dislocation core. Therefore, for emergence of pipe diffusion, the vacancies must also migrate in the direction "P2." Because the vacancy migration energy in the direction "P2" is very high (1.64 eV), it is easier for vacancies to migrate to one lower layer (LW1) (1.25 eV) and then return to the former layer (0.53 eV). Vacancy migration in the direction "UP1" is the

TABLE V. Diffusion coefficient and average migration length of pipe diffusion for 10 hours at each temperature with vacancy migration energy of 1.25 eV in Fe.

Temperature (K)	Diffusion coefficient (m^2/s)	Average migration length for 10 hours (nm)
300	2.06×10^{-28}	2.72×10^{-3}
373	2.65×10^{-24}	3.09×10^{-1}
473	9.85×10^{-21}	18.8
573	2.08×10^{-18}	2.74×10^{2}
673	8.95×10^{-17}	1.79×10^{3}

same as that in the direction "*P*1," which is the direction away from the dislocation core, and the energy of the former is higher than that of the latter. For pipe diffusion, vacancies must pass through two migration barriers (0.97 eV and 1.25 eV), and the mobility of pipe diffusion depends on the higher migration energy of 1.25 eV. Table V shows the diffusion coefficient and the average path of pipe diffusion for 10 hours at each temperature with the vacancy migration energy of 1.25 eV. From growth of helical dislocations by neutron irradiation, the distance between jogs is approximately 100 nm.[51] In the annealing at above 573 K, vacancies can be absorbed by preexisting jogs.

In the preceding section, the concentration of atoms existing in the dislocation core was given as approximately 5×10^{-5}. Because the vacancy clusters grew from two to five vacancies, one vacancy should be trapped per 33 atoms (approximately 8.3 nm) on the dislocation line, which is obtained by $5 \times 10^{-5}/[5 \times 10^{-7} \times (5-2)]$. From the second case in Table III, vacancies were trapped every eight atoms along the dislocation line at 473 K. The number of the trapped vacancies was larger than that obtained experimentally. There is a possibility that the calculated value was overestimated by the assumption of the constant vacancy concentration C_5 during annealing. A portion of the trapped vacancies may be absorbed by preexisting jogs and form jogs by binding to each other at 473 K, because of the pipe diffusion length of 18.8 nm. However, the migration energy for pipe diffusion was 1.25 eV, and that in the Burgers vector direction was between 0.07 eV and 0.64 eV. Therefore, vacancies trapped in the edge dislocations move back and forth at the dislocation core rather than along the dislocation line at below 473 K and they are detrapped and lead to the growth of the vacancy clusters at 573 K. At higher temperatures, vacancy clusters become unstable and vacancies are released

from them. These vacancies migrate to the dislocation core again. In this case, dislocations only act as a sink for vacancies and they are annihilated at jogs of the dislocations. It follows that pipe diffusion did not have any effect on the vacancy trapping and detrapping mechanism in Fe.

The vacancy formation energy in the dislocation core was 0.86 eV, and the vacancy migration energy along the dislocation line was 1.25 eV, as discussed in the preceding section. The values of the self-diffusion enthalpy along the dislocations and in the bulk were 2.11 eV (=0.86 eV +1.25 eV) and 2.48 eV (=1.70 eV+0.78 eV), respectively. Lübbehusen *et al.*[52] and Shima *et al.*[53] reported that the mobility of self-diffusion along dislocations in ultrahigh-purity Fe obtained by the radioactive tracer method was higher than that of lattice diffusion. The results of our study agreed with the results of these experiments. It was difficult for vacancies to form from the jogs at thermal equilibrium at 573 K or 673 K, since the enthalpy of the self-diffusion was high.

In Ni, the vacancy migration energies for "*P*1" and "*P*2" in Fig. 10 were 1.41 eV and 0.68 eV, respectively. In the stacking fault region far from the partial dislocations, the migration energy is 1.02 eV and lower than that in the bulk. Therefore, vacancies associated with the dislocations can migrate and vacancies tend to be annihilated at jogs. Thus, the amount of vacancies released from the dislocations at 573 K was less than in the case of α-Fe.

IV. CONCLUSION

Measurements of positron-annihilation lifetime and coincidence Doppler broadening in positron annihilation on Ni and Fe deformed at high and low speeds were performed. In these experiments, the reported existence of vacancies trapped in edge dislocations was confirmed, and vacancy detrapping from the dislocations at 473–573 K was observed for the first time. The strength of vacancy trapping and the effect of vacancy pipe diffusion were examined by computer simulation. It was concluded that pipe diffusion did not affect the mechanism of vacancy trapping and detrapping in edge dislocations. The growth of the vacancy clusters due to the detrapping of vacancies led to an increase in the positron lifetime at 473–573 K.

Our present work provides fresh evidence of the trapping and detrapping mechanism of vacancies at dislocations. This mechanism will require current theories of the sink efficiency of dislocations to be changed and the effect of dislocation bias under high-energy particle irradiation of metals to be reconsidered.

*Present address: Toyota Central R&D Labs., Inc.

[1] R. M. Thomson and R. W. Balluffi, J. Appl. Phys. **33**, 803 (1962).

[2] R. M. Thomson and R. W. Balluffi, J. Appl. Phys. **33**, 817 (1962).

[3] R. W. Balluffi and D. N. Seidman, J. Appl. Phys. **36**, 2708 (1965).

[4] R. W. Balluffi, Phys. Status Solidi **31**, 443 (1969).

[5] G. R. Love, Acta Metall. **12**, 731 (1964).

[6] R. W. Balluffi, Phys. Status Solidi **42**, 11 (1970).

[7] M. J. Turunen and V. K. Lindroos, Philos. Mag. **29**, 701 (1974).

[8] P. T. Heald, Philos. Mag. **31**, 551 (1975).

[9] R. Bullough, B. L. Eyre, and K. Krishan, Proc. R. Soc. London, Ser. A **346**, 81 (1975).

[10] E. Kuramoto, J. Nucl. Mater. **175-181**, 1019 (1991).

[11] E. Kuramoto, J. Nucl. Mater. **191-194**, 1279 (1992).

[12] E. Kuramoto and T. Tsutsumi, J. Nucl. Mater. **212-215**, 175 (1994).

[13] C. Hidalgo, G. Gonzalez-Doncel, S. Linderoth, and J. San Juan, Phys. Rev. B **45**, 7017 (1992).

[14] H. Ohkubo, Z. Tang, Y. Nagai, M. Hasegawa, T. Tawara, and M. Kiritani, Mater. Sci. Eng., A **350**, 95 (2003).

[15] H. Häkkinen, S. Mäkinen, and M. Manninen, Europhys. Lett. **9**, 809 (1989).

[16] H. Häkkinen, S. Mäkinen, and M. Manninen, Phys. Rev. B **41**, 12441 (1990).

[17] Y. Kamimura, T. Tsutsumi, and E. Kuramoto, Phys. Rev. B **52**, 879 (1995).

[18] V. R. Fidelman and V. A. Zhuravlev, Phys. Met. Metallogr. **46**, 85 (1979).

[19] J. Huang, M. Meyer, and V. Pontikis, Phys. Rev. Lett. **63**, 628 (1989).

[20] J. Huang, M. Meyer, and V. Pontikis, Philos. Mag. A **63**, 1149 (1991).

[21] V. A. Borodin, Y. R. Kevorkyan, V. V. Kolomytkin, and A. I. Ryazanov, J. Nucl. Mater. **187**, 131 (1992).

[22] J. von Boehm and R. M. Nieminen, Phys. Rev. B **50**, 6450 (1994).

[23] J. von Boehm and R. M. Nieminen, Phys. Rev. B **53**, 8956 (1996).

[24] Q. F. Fang and R. Wang, Phys. Rev. B **62**, 9317 (2000).

[25] E. Kuramoto, K. Ohsawa, T. Tsutsumi, and M. Koyanagi, J. Nucl. Mater. **271&272**, 26 (1999).

[26] E. Kuramoto, J. Nucl. Mater. **276**, 143 (2000).

[27] M. J. Puska and R. M. Nieminen, J. Phys. F: Met. Phys. **13**, 333 (1983).

[28] P. Kirkegaard, M. Eldrup, O. E. Mogensen, and N. J. Pedersen, Comput. Phys. Commun. **23**, 307 (1981).

[29] T. Ishizaki, T. Yoshiie, K. Sato, S. Yanagita, Q. Xu, M. Komatsu, and M. Kiritani, Mater. Sci. Eng., A **350**, 102 (2003).

[30] M. Kiritani, T. Sota, T. Tawara, H. Arimura, K. Yasunaga, Y. Matsukawa, and M. Komatsu, Radiat. Eff. Defects Solids **157**, 53 (2002).

[31] T. Tawara, Y. Matsukawa, and M. Kiritani, Mater. Sci. Eng., A **350**, 70 (2003).

[32] K. Yasunaga, M. Iseki, and M. Kiritani, Mater. Sci. Eng., A **350**, 76 (2003).

[33] K. W. Jacobsen, P. Stoltze, and J. K. Norskov, Surf. Sci. **366**, 394 (1996).

[34] G. J. Ackland, D. J. Bacon, A. F. Calder, and T. Harry, Philos. Mag. A **75**, 713 (1997).

[35] P. C. J. Gallagher, Mater. Trans., JIM **1**, 2429 (1970).

[36] S. Nanao, K. Kuribayashi, S. Tanigawa, and M. Doyama, J. Phys. F: Met. Phys. **7**, 1403 (1977).

[37] M. Kiritani, M. Konno, T. Yoshiie, and S. Kojima, Mater. Sci. Forum **15-18**, 181 (1987).

[38] A. Seeger and H. Kronmuller, Mater. Sci. Forum **15-18**, 65 (1987).

[39] L. De Schepper, D. Segers, L. Dorikens-Vanpraet, M. Dorikens, G. Knuyt, L. M. Stals, and P. Moser, Phys. Rev. B **27**, 5257 (1983).

[40] M. Kiritani, H. Takata, K. Moriyama, and F. E. Fujita, Philos. Mag. A **40**, 779 (1979).

[41] M. Kiritani, *Point Defects and Defect Interactions in Metals*, edited by J. Takamura, M. Doyama, and M. Kiritani (University of Tokyo Press, Tokyo, 1982), p. 59.

[42] S. Takaki, J. Fuss, H. Kugler, U. Dedek, and H. Schultz, Radiat. Eff. **79**, 87 (1983).

[43] F. Herman and S. Skillman, *Atomic Structure Calculations* (Prentice Hall, New York, 1963).

[44] E. Boronski and R. M. Nieminen, Phys. Rev. B **34**, 3820 (1986).

[45] G. E. Kimball and G. H. Shortley, Phys. Rev. **45**, 815 (1934).

[46] E. Kuramoto, T. Tsutsumi, K. Ueno, M. Ohmura, and Y. Kamimura, Comput. Mater. Sci. **14**, 28 (1999).

[47] A. S. Keh and S. Weissmann, *Electron Microscopy and the Strength of Crystals*, edited by G. Thomas and J. Washburn (Interscience, New York, 1963), p. 231.

[48] W. Brandt, in *Positron Anihilation*, edited by A. T. Stewart and L. O. Roeling (Academic, New York, 1967), p. 155.

[49] D. C. Connors and R. N. West, Phys. Lett. **30**, 24 (1969).

[50] M. Doyama, J. Phys. Soc. Jpn. **33**, 1495 (1972).

[51] T. Yoshiie, Y. Satoh, and Q. Xu, J. Nucl. Mater. **329-333**, 81 (2004).

[52] M. Lübbehusen and H. Mehrer, Acta Metall. Mater. **38**, 283 (1990).

[53] Y. Shima, Y. Ishikawa, H. Nitta, Y. Yamazaki, K. Mimura, M. Isshiki, and Y. Iijima, Mater. Trans., JIM **43**, 173 (2002).